Electronic Supplementary Information

Surface-Interactive Control of Apatite Nanoparticles with Albumin

Kazuto Sugimoto,[a, b] Ryota Akutsu,[a] Zizhen Liu,[a, c] Shimon Konosu, [a] and Motohiro Tagaya [a*]

[a] *Department of Materials Science and Bioengineering,*
Graduate School of Engineering, Nagaoka University of Technology,
1603-1 Kamitomioka, Nagaoka 940-2188, Japan.

[b] *Japan Society for the Promotion of Science (JSPS)*
Research Fellowship for Young Scientists (DC),
5-3-1 Koji-machi, Chiyoda-ku, Tokyo 102-0083, Japan.

[c] *Japan Society for the Promotion of Science (JSPS)*
Research Fellowship for Young Scientists (PD),
5-3-1 Kojimachi, Chiyoda-ku, Tokyo 102-0083, Japan

*** Author to whom correspondence should be addressed:**

Tel: +81-258-47-9345; Fax: +81-258-47-9300, E-mail: tagaya@mst.nagaokaut.ac.jp

Experimental Procedure S1

The chemical compositions of the nanoparticles after immersion in PB were measured by XRF (ZSX Primus II, Rigaku Corporation). For XRF analysis, the powders were pelleted without dilution. The basic parameter method was performed using the software for semi-quantitative analysis (EZ Scan Program, Rigaku Corporation), and the molar ratio of Ca to P was calculated based on the calibration curve.

Zeta potential values were measured using a zeta potential meter (ZETASIZER Pro, Malvern Panalytical Corporation). The nanoparticles were dispersed in PB at a concentration of 0.01 wt%, and the zeta potential was measured using electrophoretic light scattering (ELS), specifically by the laser backscattering method. The analysis was conducted using the software supplied with the instrument (Zetasizer Nano software, Malvern Panalytical Corporation).[S1]

The crystalline phase was evaluated by XRD (Smart Lab, Rigaku Corporation). The diffraction patterns were recorded using a powder X-ray diffractometer with a CuKα X-ray source. The weight concentrations of HA and α-phase tricalcium phosphate (α-TCP) were determined from the diffraction peak intensities of α-TCP and HA in the obtained patterns using the Reference Intensity Ratio (RIR) method.[S2] The analysis was performed using the software (Rigaku Corporation, software name: Smart Lab studio II).

References for this page

S1. S. Yamada, S. Motozuka and M. Tagaya, *J Mater Chem B*, 2020, **8**, 1524–1537.

S2. L. Alexander and H. P. Klug, *Anal Chem*, 1948, **20**, 886–889.

Experimental Procedure S2

For the evaluation of the hydration layer, FT-IR spectra were recorded on Fourier transform infrared spectrometer (FT/IR-4600, JASCO Co., Ltd.) using the KBr powder method, and the weight ratio of sample powder to KBr was 1:9. All the spectra were recorded after subtracting the background spectrum of KBr. The FT-IR spectral separation was performed using the same procedure described in our previous reports, and the spectra were separated as shown in **Table S1** and **S2**.[S3] To evaluate the stretching vibration state of the hydrogen bonds in the hydration layer, asymmetric stretching vibration ratio (R_{as}) was obtained from the peak area ratio of the asymmetric stretching vibration [F-1] to the symmetric stretching vibration [I], as shown in **Eq. (S1)**.

$$R_{\mathrm{as}} = \frac{[\mathrm{F\text{-}}1]\ \text{Asymmetric stretching vibration of water}}{[\mathrm{I}]\ \text{Symmetric stretching vibration of water}} \qquad (\mathbf{S1})$$

Reference for this page

S3. S. Yamada, Y. Chai and M. Tagaya, *Phys Chem Chem Phys*, 2022, **24**, 6788–6802.

Table. S1

Table S1 Peak assignment of three different hydration layers on the apatite nanoparticles in the FT-IR spectra.

Peak area number	Assignment	Peak position range / cm^{-1}
[F]	Free water	3180–3220
[I]	Intermediate water	3400–3440
[N-f]	Non-freezing water	3580–3620
[HA]	ν_s of the hydroxyl group (OH in apatite)	3570–3572

Table. S2

Table S2 Peak assignment of five different vibrational states of the hydration layers on the apatite nanoparticles in the FT-IR spectra, which were obtained by collecting the vibration components possibly interacting with the HA surfaces after precise peak separation in **Table S1**.

Peak area number	Peak assignment and type of water		Peak position range / cm^{-1}
[F-1]	Asymmetric stretching vibration of water	Free water	3170–3210
[F-2]	Deformation vibration of water	Free water	3240–3480
[I]	Symmetric stretching vibration of water	Intermediate water	3410–3450
[N-f]	Stretching vibration of water	Non-freezing water	3590–3630
[HA]	v_s of the hydroxyl group (OH in apatite)	–	3570–3572

Experimental Procedure S3

Quartz Crystal Microbalance with Dissipation (QCM-D) equipment (Biolon Scientific, Co. Ltd.: Qsense Explorer) was used to evaluate the Alb adsorption behavior. According to the previous report,[S3] the measurements were performed by monitoring Δ*f* and Δ*D* curves (**Fig.S1** and **Fig. S2**). Furthermore, the Δ*D*/Δ*f* plots, where the Δ*f* and Δ*D* were expressed as the abscissa and ordinate, respectively, were used to evaluate the adsorption behavior of Alb. To discuss the changes in the adsorption states in greater detail, the change in angle for the slopes of the Δ*D*-Δ*f* plot from (1) the initial stage and (2) the equilibrium stage. Specifically, the angles $\theta_{\text{ini.}}$ and $\theta_{\text{eq.}}$ were calculated from the slopes of $v_{\text{ini.}}$ (the initial stage) and $v_{\text{eq.}}$ (the equilibrium stage), respectively (**Fig. S3**). The rotation angle from (1) to (2) ($\Delta\theta$) was then calculated according to **Eq. (S2)**.

$$\Delta\theta = \theta_{\text{ini.}} - \theta_{\text{eq.}} \qquad (\mathbf{S2})$$

The Δ*f* and Δ*D* curves were then applied to the Voigt viscoelastic model to evaluate the viscoelasticity, considering the protein adsorption layer as a Newtonian fluid.[S4,S5] The analysis was performed using the provided software (Biolon Scientific, Co., Ltd.: Qsense Dfind), and the viscoelastic parameters such as viscosity (η_{ad}), elastic modulus (μ_{ad}), density (ρ_{ad}) and thickness (d_{ad}) of the adsorption layer were calculated by fitting the Δ*f* and Δ*D* curves to the models through the fixation of the density (ρ_{l}) and the viscosity (η_{l}) of the bulk solution.[S6-S8] The tan δ was evaluated using **Eq. (S3)** from μ_{ad} and η_{ad} obtained from the Voigt viscoelastic model and the resonance frequency (*f*).[S9]

$$\tan\delta = \frac{2\pi f \eta_{\text{ad}}}{\mu_{\text{ad}}} \qquad (\mathbf{S3})$$

References for this page

S3. S. Yamada, Y. Chai and M. Tagaya, *Phys Chem Chem Phys*, 2022, **24**, 6788–6802.

S4. F. Höök, B. Kasemo, T. Nylander, C. Fant, K. Sott and H. Elwing, *Anal Chem*, 2001, **73**, 5796–5804.

S5. M. V Voinova, M. Rodahl, M. Jonson and B. Kasemo, *Phys Scr*, 1999, **59**, 391.

S6. G. Dunér, E. Thormann and A. Dėdinaitė, *J Colloid Interface Sci*, 2013, **408**, 229–234.

S7. A. Sonoi, I. Furikado and K. Ishihara, *Langmuir*, 2021, **37**, 3897–3902.

S8. I. Furikado, J. Forsman and T. Nylander, *Anal Chem*, 2023, **95**, 15286–15292.

S9. M. Tagaya, T. Ikoma, N. Hanagata and J. Tanaka, *Mater Express*, 2012, **2**, 1–22.

Fig. S1

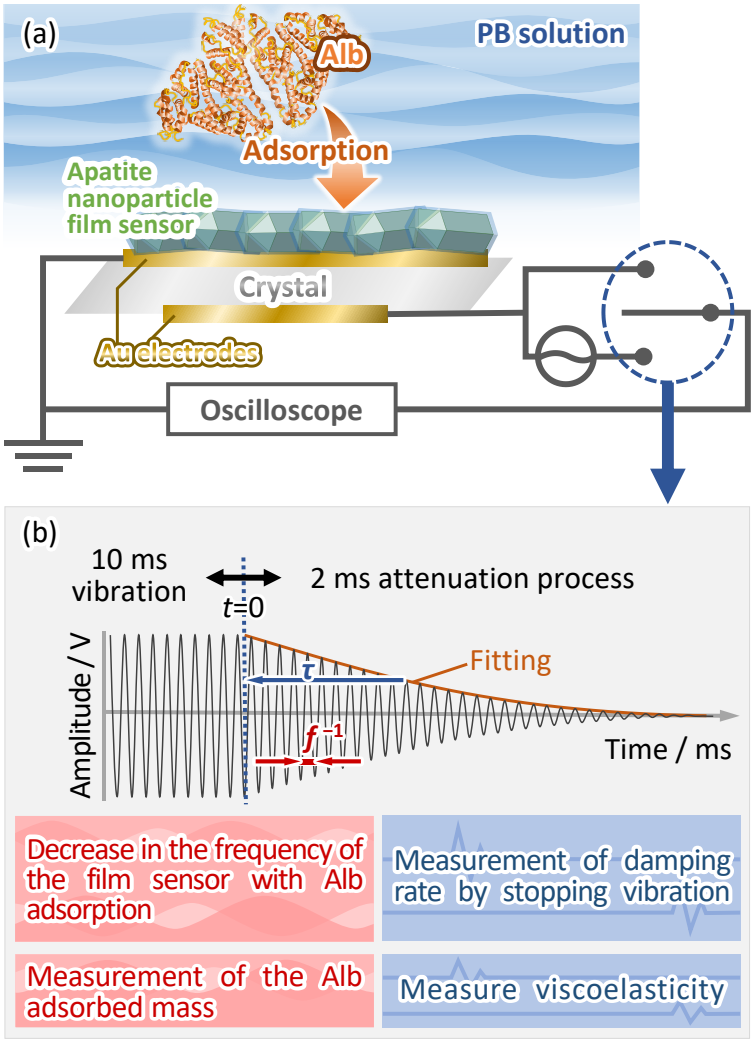

Fig. S1. Illustration of (a) measurement of Alb adsorption behavior on the apatite nanoparticles using QCM-D sensor, and (b) typical rapid excitation of the QCM-D near resonance, followed by an exponentially damped sinusoidal wave after rapid disconnection, which can be fitted to calculate τ.

Fig. S2

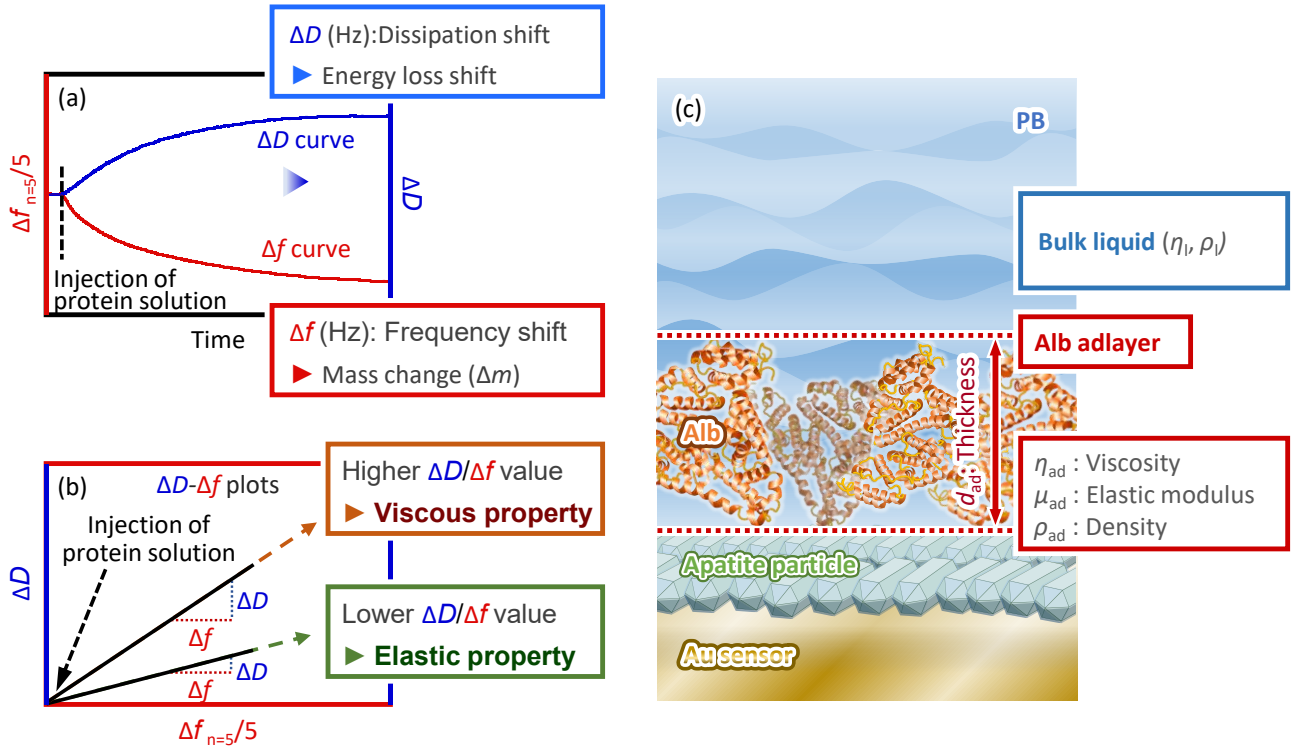

Fig. S2. Representative images of (a) Δ*D* and Δ*f* curves, and (b) the Δ*D*-Δ*f* plots. (c) Schematic illustration of the geometry and parameters used to simulate the hydrated layers and Alb adlayer on apatite nanoparticles film located between the QCM-D sensor surface and a semi-infinite Newton liquid.

Fig. S3

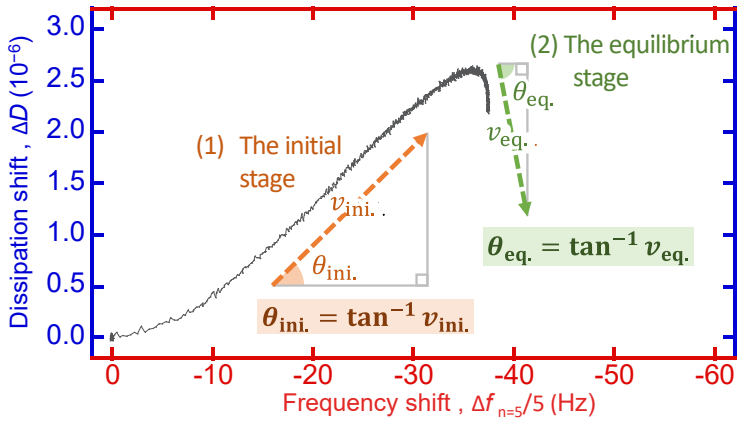

Fig. S3. Calculation method for the slope angles in (1) the initial stage and (2) the equilibrium stage in the Δ*D*-Δ*f* plot. From the $v_{ini.}$ and $v_{eq.}$ in the initial and equilibrium stages, the $\theta_{ini.}$ and $\theta_{eq.}$ in the initial and equilibrium stages were calculated as shown in inset.

Experimental Procedure S4

The aforementioned FT-IR instrument was used to evaluate the Alb adsorption layer. Since the amide I region, which reflects the secondary structure of the protein, overlaps with the O—H bending vibrational component of water, the difference spectrum between the Alb adsorbed sample (***X***-10-Alb) and the reference sample (***X***-10-PB) was prepared and analyzed (**Fig. S4**). Specifically, second-order differentiation of the amide I region was performed using the software provided with the instrument (Spectra Manager by Japan Spectroscopy Co., Ltd.), and eight peaks corresponding to protein secondary structure components were identified (**Fig. S5**). The spectral separation was then performed according to **Table S3**.[S3] Among the secondary structures, α-helix and β-sheet represent the native state of the protein, while Turn and Random are associated with the denatured state. Accordingly, the denaturation state of Alb can be evaluated from the peak area ratio of these components, as shown in **Eq. (S4)**.

$$\text{Denatured state of Alb} = \frac{Compo(\text{Turn}) + Compo(\text{Random})}{Compo(\alpha - \text{helix}) + Compo(\beta - \text{sheet})} \quad (\mathbf{S4})$$

Reference

S3. S. Yamada, Y. Chai and M. Tagaya, *Phys Chem Chem Phys*, 2022, **24**, 6788–6802.

Fig. S4

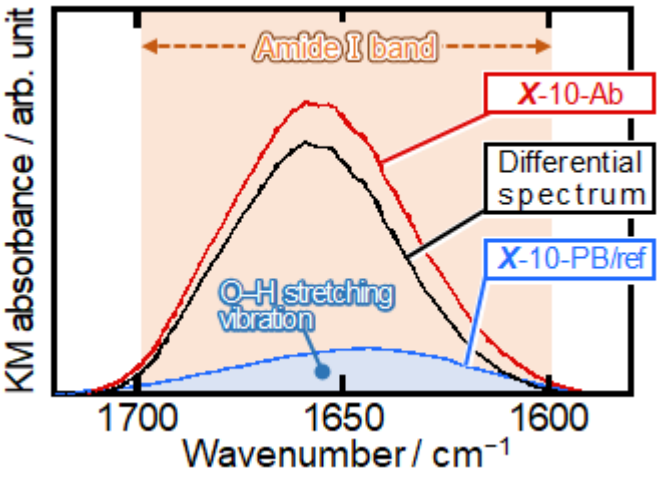

Fig. S4. Representative differential spectrum illustrating removal of O—H stretching vibration and isolation of the amide I band, obtained by subtracting the ***X***-10-PB/ref spectrum from the ***X***-10-Alb spectrum.

Fig. S5

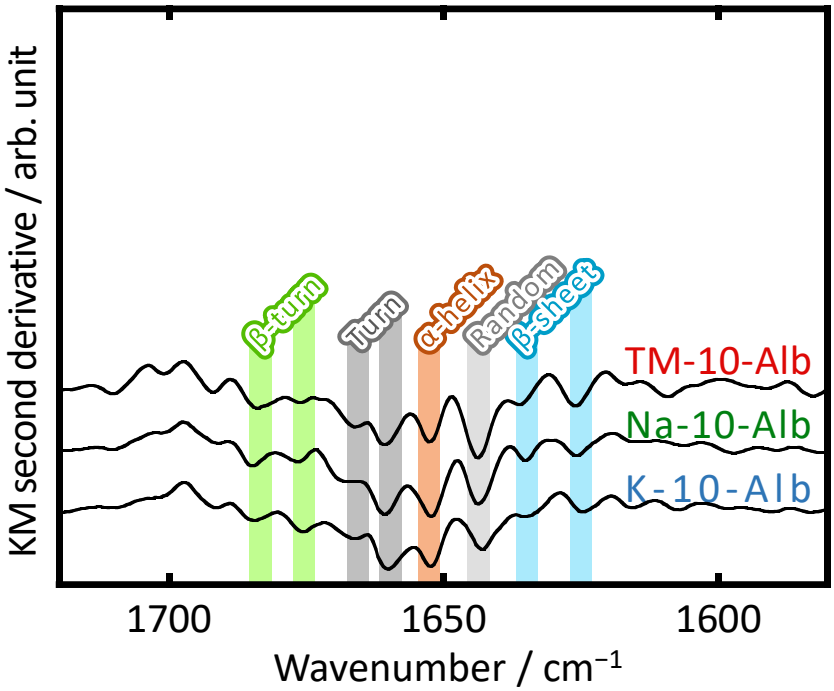

Fig. S5. Second derivatives of the FT-IR spectra in the amide I region of the Alb adlayer on the apatite nanoparticles.

Table. S3

Table S3 Peak assignment of the amide I band in the FT-IR spectra of Alb layer on the apatite nanoparticles.

Peak area number	Assignment	Peak position range / cm^{-1}
[βs-1]	β-sheet (1)	1623–1627
[βs-2]	β-sheet (2)	1633–1637
[R]	Random	1642–1646
[α]	α-helix	1651–1655
[T-1]	Turn	1658–1662
[T-2]	Turn	1664–1668
[βt-1]	β-turn (1)	1673–1677
[βt-2]	β-turn (2)	1682–1686

Fig. S6

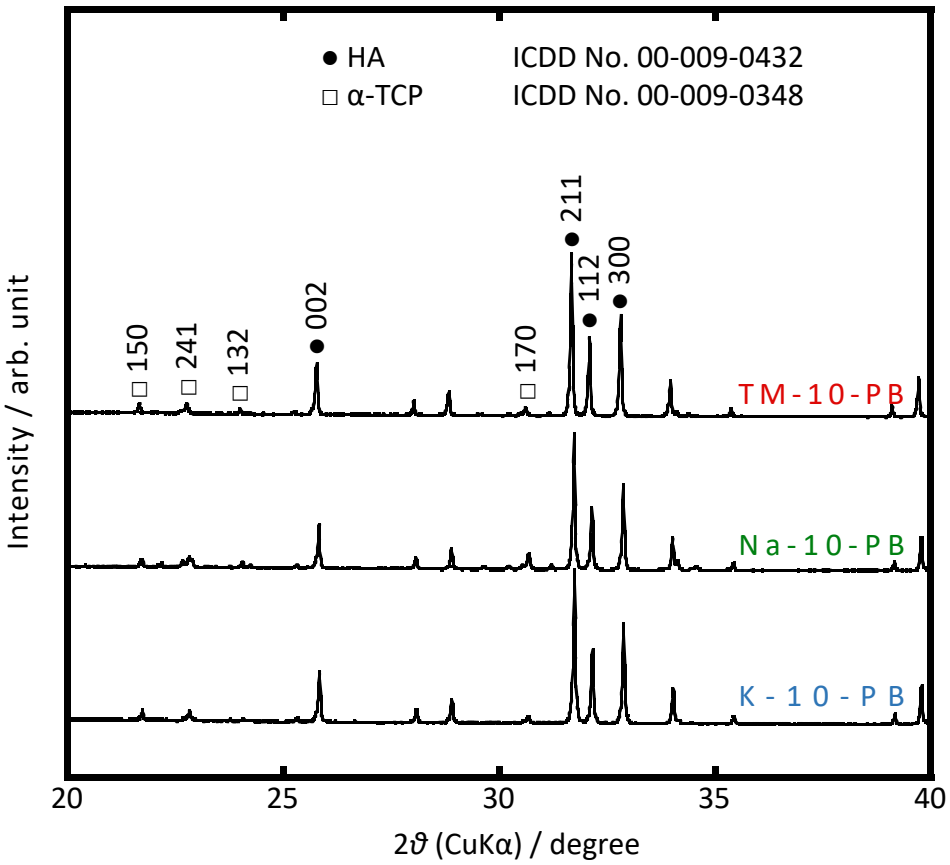

Fig. S6. XRD patterns of the apatite nanoparticles after the immersion in PB and calcination at 1200 °C.

Fig. S7

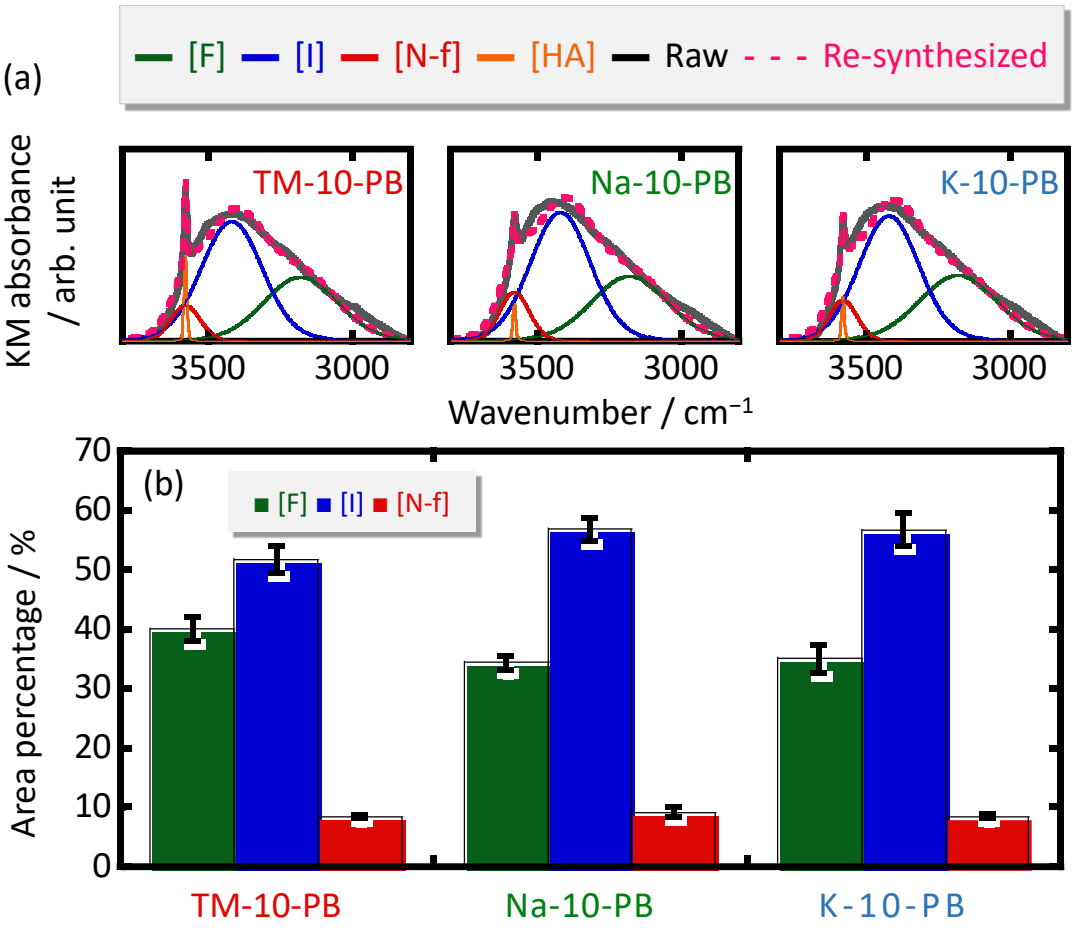

Fig. S7. (a) Curve fitting and spectral separation results of four components of the O—H absorption bands in the FT-IR spectra of the nanoparticles. The detailed assignments for ***X***-10-PB are provided in **Table S1**. (b) Area percentage of three types of hydration layers formed on the nanoparticles after immersion in PB.

Fig. S8

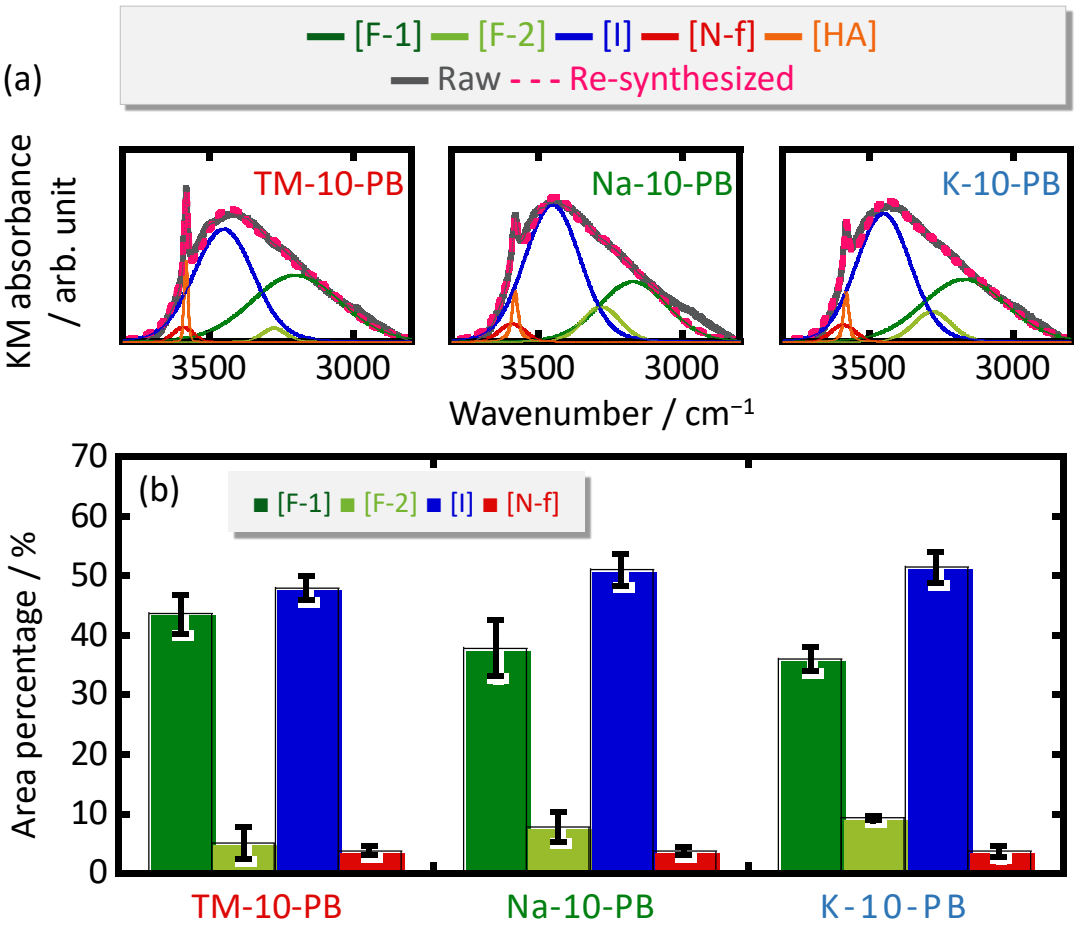

Fig. S8. (a) Curve fitting and spectral separation results of five components of the O—H absorption bands in the FT-IR spectra of the nanoparticles. The detailed assignments are provided in **Table S2**. (b) Area percentage of four types of hydration layers formed on the nanoparticles after immersion in PB.

Scheme S1

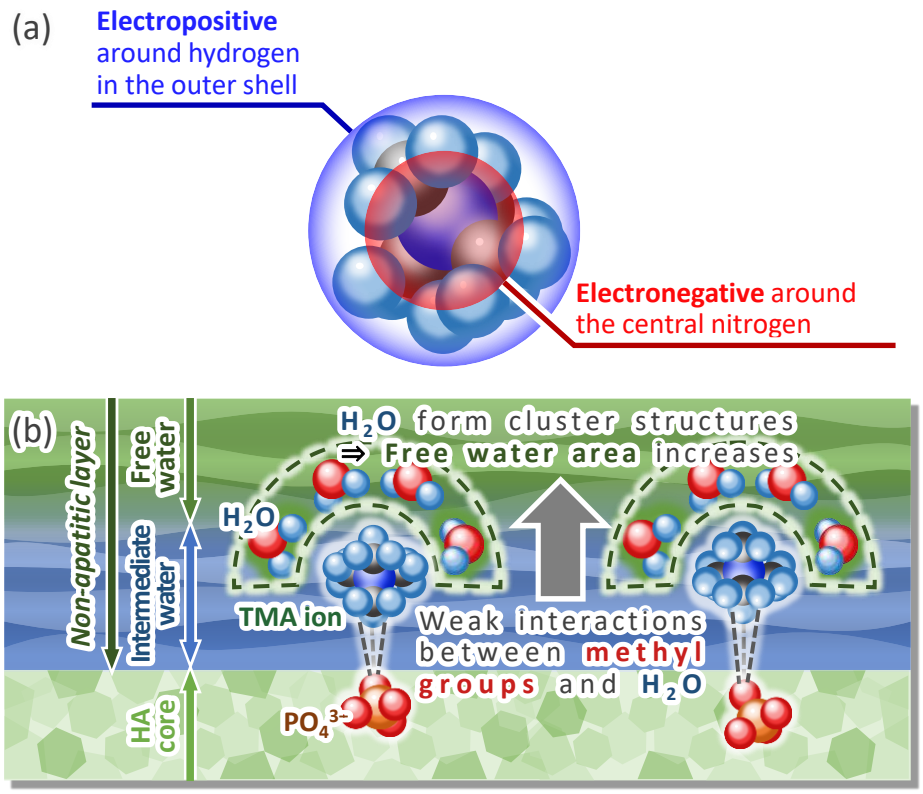

Scheme S1. Illustration of (a) the pseudospherical charge distribution of the TMA ion, and (b) the coordination states of TMA ions with phosphate ions in the HA core, estimated from the charges and H_2O states.

Fig. S9

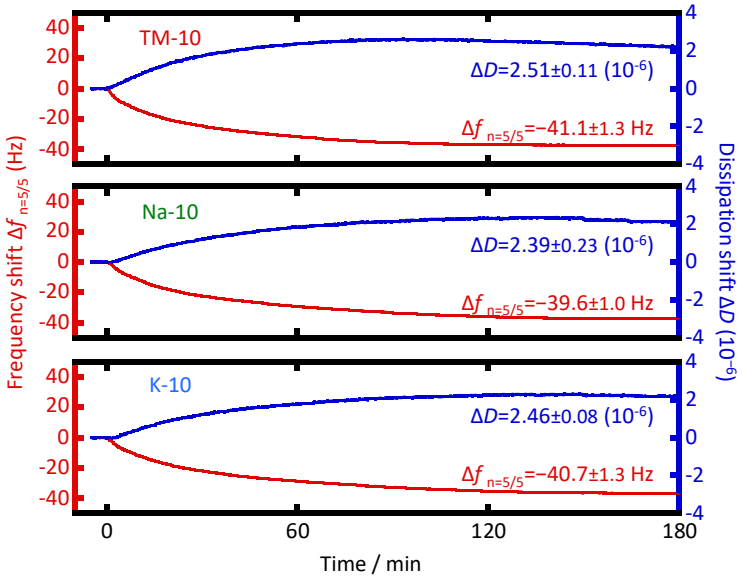

Fig. S9. Δ*D* and Δ*f* curves with the Alb adsorption on the nanoparticle films.

Fig. S10

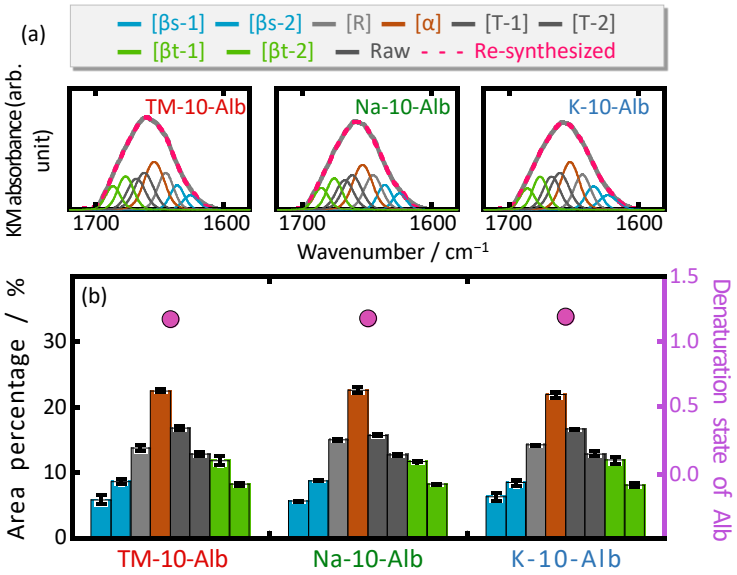

Fig. S10. (a) Curve fitting and spectral separation results of seven components of the amide I bands of the nanoparticles in the FT-IR spectra. The detailed assignments are provided in **Table S3**. (b) Area percentages of secondary structure components in the Alb adsorption layer obtained from (a), and the degree of Alb denaturation calculated from **Eq. (S3)**. Reference values of secondary structure percentages in solution: α-helix=54.7%, β-sheet=6.7%, Random=19.8%, β-turn=7.6%.

Scheme S2

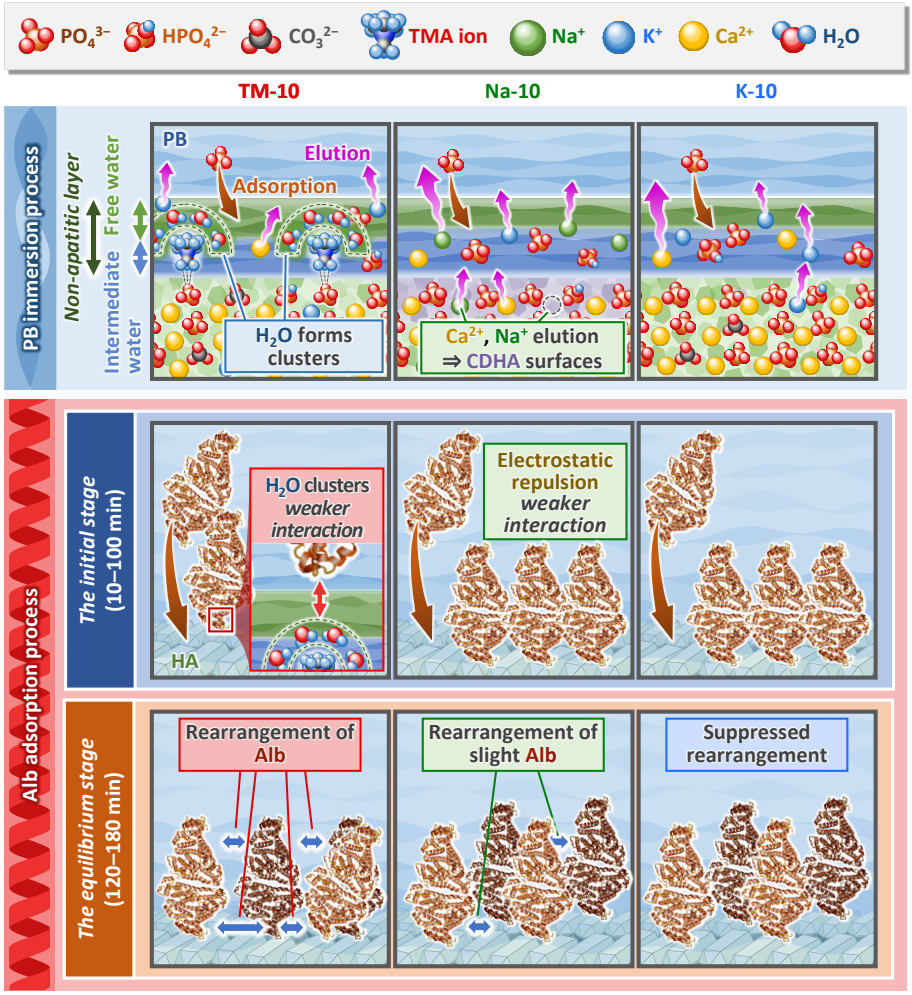

Measured value	TM-10	Na-10	K-10
Zeta potential / mv	−25.5±0.4	−27.2±0.4	−24.9±0.1
$\Delta D/\Delta f$ rotation angle $\times 10^{-7}$ / °	−76.9±17.3	−38.1±13.8	−9.2±1.4
tanδ / -	2.67±0.34	1.71±0.13	1.54±0.12
Alb layer thickness / nm	12.1±0.8	12.1±0.4	11.4±0.5
α-helix percentage / %	22.5±0.2	22.6±0.5	21.9±0.4

Scheme S2. Illustration of the changes in the surface states of the nanoparticles during the PB immersion and the initial and equilibrium stages of the Alb adsorption, which were supported by the measured values in this study.